Contents lists available at ScienceDirect

EBioMedicine

Research paper

Novel theranostic agent for PET imaging and targeted radiopharmaceutical therapy of tumour-infiltrating immune cells in glioma

Alexandra Foster[1,a], Shubhanchi Nigam[1,b], David S Tatum[c], Itay Raphael[a], Jide Xu[c], Rajeev Kumar[a], Elizabeth Plakseychuk[d], Joseph D Latoche[d], Sarah Vincze[a], Bo Li[a], Rajan Giri[e], Lauren H McCarl[a], Robert Edinger[b], Murat Ak[b], Vishal Peddagangireddy[b], Lesley M Foley[f], T Kevin Hitchens[f,g], Rivka R Colen[b], Ian F Pollack[a], Ashok Panigrahy[b], Darren Magda[c,*], Carolyn J Anderson[b,d,h,i,j,k,*,#], W Barry Edwards[b,e,*], Gary Kohanbash[2,a,l,*]

[a] Department of Neurological Surgery, University of Pittsburgh, Pittsburgh, PA 15213, USA
[b] Department of Radiology, University of Pittsburgh, Pittsburgh, PA 15213, USA
[c] Lumiphore, Inc., 600 Bancroft Way Berkeley, CA 94710, USA
[d] Department of Medicine, University of Pittsburgh, Pittsburgh, PA 15213, USA
[e] Department of Biochemistry, University of Missouri, Columbia, MO, 65211, USA
[f] Animal Imaging Center, University of Pittsburgh, Pittsburgh, PA 15213, USA
[g] Department of Neurobiology, University of Pittsburgh, Pittsburgh, PA 15213, USA
[h] Department of Bioengineering, University of Pittsburgh, Pittsburgh, PA 15213, USA
[i] Department of Pharmacology & Chemical Biology, University of Pittsburgh, Pittsburgh 15213, USA
[j] Department of Chemistry, University of Pittsburgh, Pittsburgh, PA 15213, USA
[k] Department of Chemistry, University of Missouri, Columbia, MO, 65211 USA
[l] Department of Immunology, University of Pittsburgh, Pittsburgh, PA 15213, USA

ARTICLE INFO

ABSTRACT

Background: Malignant gliomas are deadly tumours with few therapeutic options. Although immunotherapy may be a promising therapeutic strategy for treating gliomas, a significant barrier is the CD11b⁺ tumour-associated myeloid cells (TAMCs), a heterogeneous glioma infiltrate comprising up to 40% of a glioma's cellular mass that inhibits anti-tumour T-cell function and promotes tumour progression. A theranostic approach uses a single molecule for targeted radiopharmaceutical therapy (TRT) and diagnostic imaging; however, there are few reports of theranostics targeting the tumour microenvironment.

Methods: Utilizing a newly developed bifunctional chelator, Lumi804, an anti-CD11b antibody (αCD11b) was readily labelled with either Zr-89 or Lu-177, yielding functional radiolabelled conjugates for PET, SPECT, and TRT.

Findings: ^{89}Zr/^{177}Lu-labeled Lumi804-αCD11b enabled non-invasive imaging of TAMCs in murine gliomas. Additionally, ^{177}Lu-Lumi804-αCD11b treatment reduced TAMC populations in the spleen and tumour and improved the efficacy of checkpoint immunotherapy.

Interpretation: ^{89}Zr- and ^{177}Lu-labeled Lumi804-αCD11b may be a promising theranostic pair for monitoring and reducing TAMCs in gliomas to improve immunotherapy responses.

Funding: A full list of funding bodies that contributed to this study can be found in the Acknowledgements section.

* Co-corresponding author.
E-mail addresses: dmagda@lumiphore.com (D. Magda), Carolyn.j.anderson@missouri.edu (C.J. Anderson), wbe59z@missouri.edu (W.B. Edwards), gary.kohanbash2@chp.edu (G. Kohanbash).
[1] Co-first author; authors contributed equally
[2] Lead contact
Current affiliation: **Wilson B Edwards, PhD:** University of Missouri; Department of Biochemistry, Chemistry, and Radiology, 222 Schweitzer Hall, Columbia, MO 65211. Tel: (573) 882-4845. **Carolyn J Anderson, PhD:** University of Missouri; Departments of Chemistry and Radiology, 1514 Research Park Drive, Columbia, MO 65211. Tel: (573) 882-8374.

1. Introduction

Gliomas are the most common primary malignant brain tumour [1]. The current standard of care for gliomas includes a combination of surgery, chemotherapy, and radiation therapy, depending on the specific type of tumour. However, even with current treatments, the median survival times for patients with high-grade gliomas (HGG), including the World Health Organization (WHO) grade IV glioma

Research in context

Evidence before this study

A theranostic approach that uses a single molecule for targeted radiopharmaceutical therapy (TRT) and diagnostic imaging could improve outcomes for malignant glioma by quantifying a pool of immunosuppressive cells bearing the biomarker CD11b and selectively targeting eradication of those cells.

Added value of this study

A single molecule, Lumi804-anti-CD11b, labelled with either ^{89}Zr or ^{177}Lu, enabled non-invasive imaging of TAMCs in murine gliomas. Additionally, ^{177}Lu-Lumi804-anti-CD11b treatment reduced TAMC populations in the spleen and tumour and improved the efficacy of checkpoint immunotherapy.

Implications of all the available evidence

Together, ^{89}Zr- and ^{177}Lu-labeled Lumi804-αCD11b may be a promising theranostic pair for monitoring and reducing TAMCs in gliomas to improve immunotherapy responses.

(glioblastoma), have held steady at approximately 15 months in both adults and children [1,2]. Therefore, more effective treatment approaches are urgently needed.

Theranostics are agents that enable both therapy and diagnostic imaging utilizing a single targeting molecule (e.g. an antibody or peptide). Recent theranostics have incorporated radiometals for PET imaging and targeted radiopharmaceutical therapy (TRT) [3,4]. For example, DOTA-octreotate (dotatate) radiolabelled with Lu-177 (^{177}Lu-dotatate; Lutathera) or Ga-68 (^{68}Ga-dotatate; NetSpot) are FDA-approved for TRT and PET imaging, respectively [5,6], emphasizing the translational potential of theranostic agents with a single chelator for both therapy and PET.

Preclinical and clinical studies support the safety and early efficacy of immunotherapies for gliomas in both adults and children. However, the immunosuppressive tumour microenvironment (TME), largely mediated by CD11b$^+$ tumour-associated myeloid cells (TAMCs), remains a barrier to successful glioma immunotherapy. In fact, CD11b$^+$ myeloid-derived cells are the predominant subset of non-malignant cells in the glioma TME. These cells are considered as a high priority target for glioma treatment and improving immunotherapy responses [7,8]. TAMCs include subpopulations of tumour-associated macrophages (TAMs) and myeloid-derived suppressor cells (MDSCs), which together account for up to 40% of a glioma's mass [9,10] and are associated with decreased survival [11,12]. Additionally, TAMCs express many inhibitory molecules that promote tumorigenesis, maintain the immune-suppressive TME, and suppress T-cell mediated anti-tumour immunity [13]. Recent translational research efforts targeting TAMCs have focused on blocking specific TAMC-expressed cell mechanisms including colony-stimulating factor 1 receptor (CSF-1R), CD47 signalling pathways, and immune-checkpoint molecules such as programmed cell death 1/programmed cell death ligand 1 (PD-1/PD-L1) [14-17]. Importantly, decreased TAMC levels in murine gliomas are associated with extended survival times [17]. Thus, selective eradication of these cells may improve patient overall survival as well as response to immunotherapy [13,18]. Moreover, monitoring TAMC levels within the glioma TME is essential to assess the efficacy of TAMC-targeted therapies. Along this line, since CD11b is a predominant marker expressed by cells of the myeloid lineage including TAMCs, previous reports of immunoPET of CD11b have shown promising results in assessing myeloid cell levels in bone marrow, spleen, and gut in murine models of colitis,

melanoma, and systemic inflammation [19-21]. We previously showed that ^{89}Zr-DFO-αCD11b exhibits high tumour uptake and enables visualization of TAMCs in an orthotopic syngeneic mouse glioma using preclinical immunoPET imaging [22], thus demonstrating the potential of ^{89}Zr-αCD11b conjugates to monitor CD11b levels in the central nervous system (CNS) within the glioma TME. The high tumour uptake of ^{89}Zr-DFO-αCD11b, coupled with the critical importance of targeting TAMCs, led us to hypothesize that an anti-CD11b antibody conjugate could be developed into an immuno-theranostic for gliomas. However, while Zr-89 is a positron emitter useful for immunoPET diagnostic agents, it lacks cytotoxicity appropriate for TRT. We therefore selected Lu-177, a clinically relevant cytotoxic β^- emitter, to target TAMCs and TAMC-adjacent cancer cells with TRT.

As bifunctional chelators (BFCs) that can bind both Zr-89 and Lu-177 radionuclides are not available, we report here on the use of a new macrocyclic BFC, Lumi804, developed for that purpose which thus may facilitate translation. Moreover, we evaluated the immuno-theranostic targeting of TAMCs in a murine glioma model using an anti-CD11b antibody (αCD11b) conjugated to Lumi804 for the use of both TRT and immuno-PET. We showed that Lumi804 rapidly and stably chelates both Zr-89 and Lu-177 at ambient temperature, which is an essential feature for radiolabelling a heat-sensitive antibody-based theranostic agent. The data presented here suggest ^{89}Zr/^{177}Lu-Lumi804-αCD11b can be used as novel immuno-theranostic agent for gliomas, which can both improve immunotherapy responses (Lu-177) while visualizing response to therapy (Zr-89).

2. Methods

2.1. Reagents

Chemicals were purchased from Sigma-Aldrich unless otherwise specified. Antibodies for flow cytometry and αCD11b (clone M1/70) were purchased from BioLegend. Immune checkpoint inhibitor antibodies, αPD-1 (clone RMP1-14) and αCTLA-4 (clone 9H10), were purchased from BioXCell. The deferoxamine (DFO) BFC (p-NCS-Bz-DFO) was purchased from CheMatech. Ca-Lumi804-NHS was prepared as previously described. Zirconium-89 oxalate was purchased from the University of Wisconsin. Lutetium-177 chloride was obtained from the Department of Energy National Isotope Development Center. Lumi804 is a proprietary bifunctional chelator patented by Lumiphore.

2.2. Instrumentation and software

Radiochemistry reaction progress and yield were monitored using an Agilent 1260 infinity HPLC (Agilent Technologies) equipped with a Superose^{TM} 12 10/300 GL SEC column (GE Healthcare). Immunoreactivity and biodistribution samples were counted using a PerkinElmer 2470 WIZARD2 Automatic Gamma Counter. Flow cytometry studies were performed on a BD LSRII (BD Biosciences), and data were analysed using FlowJo software (version 10.6.1, FlowJo, LLC). T2-weighted MRI scans were acquired with a multi slice RARE sequence using a 7T/30cm Bruker Biospec AVANCE 3 scanner equipped with a 12-cm gradient set, 40mm quadrature birdcage RF resonator with custom mouse bed and ParaVision 6.0.1 (Bruker BioSpin, Billerica MA). Tumour volumes were determined by manual segmentation using ITK-SNAP (version 3.8.0) and DSI Studio software. PET and T2-weighted MRI scans were co-registered using 3D Slicer (version 4.10.2). PET/CT and SPECT/CT scans were performed on Inveon Preclinical Imaging Stations (Siemens Medical Solutions) with Inveon Research Workstation (IRW) software (version 4.2, Siemens Healthcare, Germany). Complete blood count (CBC) studies were performed using the Abaxis Vetscan HM5 Hematology Analyzer (Allied Analytic).

2.3. Preparation of Lumi804-αCD11b and DFO-αCD11b conjugates

Aliquots of αCD11b (1.00 mL, 10.1 mg/mL stock) were buffer exchanged using size exclusion columns (SEC) prepared with sodium carbonate buffer (100 mM, pH 9.0) and Sephadex G50 Fine (GE Healthcare), and the combined eluents were quantified by UV-vis spectroscopy (ε^{280}=1.33 mL/mg). Aliquots of the resulting αCD11b solution (1 mL, 7.34 mg/mL in sodium carbonate buffer) were treated with Ca-Lumi804-NHS (16.4 μL of 4.48 mM stock solution in anhydrous DMF, 1.5 molar equivalents) and shaken at 1000 rpm on a microtube shaker for 1h. The calcium complex of Lumi804 was used in the conjugation reaction to prevent reaction of the NHS ester with the hydroxyls of the chelator (**Fig. 1**) [23]. The reaction mixture was applied to SECs prepared using TBS buffer (tris buffered saline, 50 mM Tris, 150 mM NaCl, pH 7.6) and Sephadex G50 Fine. The eluents of the SECs were combined, and a volume of CaCl$_2$ (100 mM stock solution in water) was added to bring the final concentration of Ca(II) to 1 mM. The antibody conjugate solution was quantified using UV-vis spectroscopy (Ca-Lumi804 $^{385}\varepsilon$ = 14,000 M^{-1} cm^{-1}, A_{385}/A_{280} = 1.3). The final concentration was 8.07 mg/mL (53.8 μM), with degree of labelling (DOL) = 1.29 and a ligation efficiency of 86%. The conjugate solution was sterile filtered (0.2 μm PES syringe filter) prior to use. The amount of aggregated antibody conjugate (<0.4%) was determined using SEC-HPLC (Agilent BioSEC-3 column, 3 μm, 7.8 × 300 mm, 300Å, in PBS). DFO-αCD11b was synthesized as previously described [24].

2.4. Binding assay for Lumi804-αCD11b antibody

To determine the equilibrium dissociation constant of the Lumi804-αCD11b conjugate, saturation binding assays were performed on the murine monocyte/macrophage cell line J774A.1 (ATCC, TIB-67). Thirty thousand cells/well were added to a microtiter plate (Costar 3917) treated with poly-D-lysine (6.4 μg/mL, 50 μL/well, 18 h, Advanced Biomatrix 5049). After 48 h, Fc receptors were blocked with TruStain fcX (100 nM anti-CD16/32, BioLegend, cat#101302, 20 μL/well) and cells were treated with either αCD11b (20 μL/well, 7.5 μM), to determine non-specific binding, or vehicle control (50 mM HEPES, 150 mM sodium chloride, pH 7.4) and incubated for 30 min at 37°C followed by 15 min at 4°C. After incubation, Eu-Lumi804-αCD11b (prepared by adding 3 μL 0.5 mM europium chloride to 10 mL 90 nM Ca-Lumi804-αCD11b) was added at varying concentrations to the plate and incubated (1 h, 4°C). The cells were rinsed thrice (cold HBSS), and time-resolved luminescence was measured on a microplate reader (Perkin Elmer Envision 2104, Wallac TRF europium settings). Background luminescence was subtracted from all wells, and non-specific binding was subtracted from total binding and fit by non-linear regression ($y = B_{max}$ * [conjugate] / (K_d + [conjugate]), where y is mean luminescence (AU), B_{max} is maximal luminescence, and K_d is the dissociation constant). K_d is reported as the mean ± standard deviation using values obtained from three microplates.

2.5. Radiolabelling of DFO- and Lumi804-αCD11b with Zr-89 and Lu-177

^{89}Zr-DFO-αCD11b was prepared and its purity determined by SEC-HPLC as previously described [24]. For radiolabelling of Lumi804-αCD11b, the antibody (10 nmol, 187 μL) was added to Zr-89 oxalate (111 MBq, 20 μL) or Lu-177 chloride (111 MBq, 7 μL) in 0.5 M ammonium acetate buffer pH 5.0 (200 μL) with gentisic acid (56 mM stock solution, 2 μL) and incubated for 30 min at 25 °C (Fig. 1). For all radiolabelled antibody conjugates, determination of radiochemical yield was performed by first diluting a small aliquot of the reaction mixture with 50 mM DTPA, pH 5.5, and then monitoring the reaction progress by SEC-HPLC (Superose, PBS, 0.6 mL/min).

Radiochemical yield for all conjugates was ≥ 99% with a molar activity of 11.1 GBq/μmol. Radiolabelling with high molar activities 22.2 GBq/μmol and 33.3 GBq/μmol was also achieved for ^{177}Lu-Lumi804-αCD11b with ≥ 99% radiochemical yield. Serum stability of both ^{89}Zr- or ^{177}Lu-Lumi804-αCD11b Lumi804-αCD11b (n=2 each) was monitored by radio-SEC-HPLC (Superose 6 Increase (Cytiva), 10/300, 1 mL/min, PBS) over time (24, 48, 72, 96 h) in mouse serum. For *in vivo* studies, the radiolabelled antibody conjugates were diluted in the sterile saline before i.v. injections.

2.6. Immunoreactivity assay for ^{89}Zr- and ^{177}Lu-Lumi804-αCD11b antibodies

RAW264.7 cells (ATCC, $\sim$1 × 10^6) in PBS (500 μL) were incubated with $\sim$25,000 CPM (10 μL) ^{89}Zr- or ^{177}Lu-Lumi804-αCD11b in saline for 1 h at room temperature with and without a blocking dose (100 μg αCD11b) and then centrifuged at 1500 rpm for 5 min to separate cell-bound vs. unbound radiolabelled αCD11b. Cells were washed twice with PBS, and the CPM of the supernatant and cell pellet were quantified by gamma counting for each radiolabelled conjugate. The cell-bound: supernatant ratio was used to determine the percentage of bound radiotracer (CPM $_{Pellet}$ / (CPM $_{Pellet}$ + CPM $_{supernatant}$ + CPM $_{washes}$) x 100). Total binding was corrected with non-specific binding to compute immunoreactivity.

2.7. Mouse syngeneic glioma model

The murine immunocompetent glioma 261 (GL261) model was used as previously described [22]. GL261 cells were obtained from the Division of Cancer Treatment and Diagnosis (DCTD) tumour repository of the National Cancer Institute (NCI). Cells were tested for mycoplasma periodically and prior to tumour injections. Intracranial injections of GL261 cells were performed on 5-6-week-old female C57BL/6j mice (Jackson Labs). Mice received intracranial injection of 1 × 10^5 GL261 cells at coordinates +2.50 mm medial/lateral, +1.50 mm anterior/posterior, and -3.50 mm dorsal/ventral from the bregma.

2.8. SPECT/CT, PET/CT, and biodistribution studies

SPECT/CT was performed at 24, 48 and 72 h post-i.v. injection of ^{177}Lu-Lumi804-αCD11b (100 μg, 7.4 MBq; molar activity: 11.1 GBq/μmol). ^{177}LuCl$_3$ (3.7 MBq) was used for SPECT scanner signal calibration. For PET/CT imaging, mice were injected i.v. with ^{89}Zr-Lumi804-αCD11b (50 μg, 3.7 MBq; molar activity: 11.1 GBq/μmol). For blocking studies, ^{89}Zr-Lumi804-αCD11b was co-injected with 500 μg of αCD11b antibody (unlabelled) to reduce molar activity 10-fold (1.1 GBq/μmol). ^{89}Zr-Lumi804-αCD11b uptake is expressed as SUV$_{mean}$.

Biodistribution studies of ^{89}Zr-Lumi804-αCD11b and ^{177}Lu-Lumi804-αCD11b were performed immediately after the 72h imaging. Mice were euthanized, major organs were collected, weighed, and the tissue-associated radioactivity was assessed in a gamma counter and expressed as % ID/g. The biodistribution of ^{89}Zr-Lumi804-αCD11b was also compared with that of ^{89}Zr-DFO-αCD11b at 216 h post injection. To determine the biodistribution of ^{89}Zr-DFO-αCD11b, serial PET imaging studies were performed at 1, 24, 48, 72, and 96 hours. Regions of interest were drawn around the tumour and within the contralateral brain, along with muscle, liver, and heart as a surrogate for blood. The SUVmean values were calculated (Vivo-Quant 2020, Invicro) and plotted against time.

2.9. Flow cytometry

For *ex vivo* analysis of immune cell populations, randomized day 7 glioma-bearing mice were treated with a single i.v. dose of Lumi804-αCD11b (100 μg) labelled with either 14.8 or 22.2 MBq Lu-177. At

72 h post TRT, glioma-bearing mice were euthanized, and the tumour region was harvested, dissected, and processed for flow cytometry analysis as previously described [24]. Dissociated tumour cells were incubated in TruStain fcX at 1 μg/5 $\times$ 10^6 cells and isolated splenocyte cells at 0.5 μg/5 $\times$ 10^4 cells in 100 μL staining buffer for 10 min on ice. Suspensions were then stained with 1 μL of each of the following fluorescent-labelled antibodies (Biolegend): CD45-PerCP (clone 30-F11), CD11b-AF488 (M1/70), Gr1-APC (RB6-8C5), and CD14-PE (sa14-2) or CD45-PerCP/Cy5.5, CD3-APC (17A2), CD4-PE/Cy7 (GK1.5), and CD8-PE (53-617) for 30 min at 4°C. After staining, cells were fixed with Fixation Buffer (BioLegend) and resuspended in Cyto-Last Buffer (BioLegend) for flow cytometry according to the manufacturer's protocol.

2.10. Targeted radiopharmaceutical therapy (TRT)

For survival studies, at 6 days after tumour cell injections mice were randomized for treatment (day 0). Mice received vehicle (control), two i.v. doses of Lumi804-αCD11b (100 μg) labelled with 7.4 MBq Lu-177 (TRT; days 0 and 7), i.p. injections of 200 μg of each αCTLA-4 and αPD-1 immune checkpoint inhibitors [25] on days 0, 3, 7, and 10, or combination TRT and ICI. MRI was performed one day before treatment to verify solid tumour formation and again on day 16 to quantify tumour volume (DSI Studio software). CBC analysis was performed on day 15 (after treatment). Whole blood (50-500 μL) was harvested by inserting a 4 mm GoldenRod lancet (Fisher Scientific) into the superficial temporal vein and collecting it directly into a potassium-EDTA treated Sarstedt CB300 capillary tube (Fisher Scientific). Samples were mixed and analysed on an Abaxis Vetscan HM5 Hematology Analyzer to acquire red blood cell parameters and 3-part white cell differentials. Mice were monitored for symptom-free survival (SFS) and were euthanized if >20% weight loss and neurological symptoms were observed.

2.11. Ethic statement

All animal experiments were conducted in compliance with Institutional Animal Care and Use Committee (IACUC) approved protocol #19126346 of the University of Pittsburgh.

2.12. Statistics

Statistical significance of the SUV mean and % ID/g between the mice groups were calculated using a Student's unpaired t-test. A one-way ANOVA with multiple comparisons was used to determine significance of the therapeutic efficacy and CBC data between groups of mice. Symptom-free survival (SFS) was evaluated by Kaplan Meier analysis with a log-rank test. Data are represented as the mean $\pm$ SD. Statistical significance was considered as *p<0.05, **p<0.01, and ***p<0.0001. All analyses were performed using Prism software v8.00 (GraphPad).

2.13. Role of the funding source

3. Results

3.1. Lumi804-αCD11b is radiolabelled with Zr-89 or Lu-177 at room temperature and demonstrates robust serum stability

An ideal radionuclide combination for antibody-based theranostics is Zr-89 (for PET) and Lu-177 (for TRT) due to relatively long half-lives ($t_{1/2}$: Zr-89 = 78 h; Lu-177 = 6.7 d), which are compatible with relatively slow antibody localization and clearance rates [26-29]. The recently developed BFC, Lumi804, contains an active ester for conjugation to ε-amino groups of lysine and the N-terminal amines of an antibody. Lumi804 is an octadentate, macrocyclic compound based on four 1-hydroxypyridin-2-one (1,2-HOPO) coordinating units suitable to bind both Zr-89 and Lu-177 (**Fig. 1; left panel**).

To synthesize ^{177}Lu/^{89}Zr-Lumi804-αCD11b, Ca-Lumi804 was conjugated with αCD11b to generate Ca-Lumi804-αCD11b, followed by trans-chelation of Ca(II) with Zr-89 or Lu-177 to generate the final radioactive immuno-theranostic agents (**Fig. 1**). The molar ratio of Lumi804:αCD11b was found to be 1.3 by UV-vis spectroscopy. We did not observe any degradation or aggregation of Lumi804-αCD11b within 20 days. First, we demonstrated that the photoluminescent Eu-Lumi804-αCD11b agent bound CD11b with high affinity (K_d = 2.6 nM; **Supplementary Fig. 1**). We then tested the labelling conditions for Ca-Lumi804-αCD11b with both Zr-89 and Lu-177 and achieved facile labelling at room temperature in high radiochemical yields and purity (>99% by size-exclusion chromatography-high performance liquid chromatography (SEC-HPLC)) with 11.1 GBq/μmol molar activity at end-of-synthesis for both agents (**Supplementary Fig. 2**).

To establish serum stability, we evaluated the stability of ^{89}Zr-Lumi804-αCD11b and ^{177}Lu-Lumi804-αCD11b at 37°C daily for 96 hours. Both agents demonstrated high stability (> 98%) with no evidence of radionuclide dissociation, proteolysis, or antibody aggregation at any timepoint evaluated (**Supplementary Fig. 3**). The immunoreactive fractions of ^{89}Zr-Lumi804-αCD11b and ^{177}Lu-Lumi804-αCD11b were 82% $\pm$4.1% and 69% $\pm$3.1%, respectively. Together, these data demonstrate that Ca-Lumi804-NHS is readily conjugated to the αCD11b antibody, and this conjugate can be radiolabelled with Lu-177 and Zr-89 in high radiochemical yield, purity, molar activity, and immunoreactivity at ambient temperatures.

3.2. ^{89}Zr-Lumi804-αCD11b demonstrates receptor-mediated tumour localization within glioma bearing mice

The GL261 orthotopic C57BL/6j-syngeneic glioma model is widely used for preclinical testing of immunotherapies and exhibits robust TAMC accumulation, similar to that of patient gliomas [30-32]. A limitation of many radiometal ion chelates, including Zr-89 bound to the widely used DFO chelator, is poor in vivo stability, which leads to free radionuclide uptake in the bone [29,33]. To evaluate the in vivo stability of Lumi804 with Zr-89, the biodistribution of ^{89}Zr-Lumi804-αCD11b was compared with ^{89}Zr-DFO-αCD11b at 216 h post injection into GL261-glioma bearing mice (**Fig. 2**). Blood clearance of ^{89}Zr-DFO-αCD11b (0.09 $\pm$ 0.03 %ID/g) was significantly different from ^{89}Zr-Lumi804-αCD11b (0.01 $\pm$ 0.005 %ID/g; p<0.01, unpaired Student's t-test), and higher retention in bone was observed for ^{89}Zr-DFO-αCD11b (6.3 $\pm$ 2.3 %ID/g) compared with ^{89}Zr-Lumi804-αCD11b (0.50 $\pm$ 0.05; p<0.01, unpaired Student's t-test), putatively due to accumulation of released free Zr-89. ^{89}Zr-DFO-αCD11b accumulation was also significantly higher in the kidney (2.6 $\pm$ 1.9 %ID/g) and intestine (1.2 $\pm$ 0.5 %ID/g) compared to ^{89}Zr-Lumi804-αCD11b (0.5 $\pm$ 0.03 %ID/g, p<0.01 and 0.05 $\pm$ 0.02 %ID/g, p<0.01, respectively. Unpaired Student's t-test was used), suggesting renal and hepatobiliary excretion of ^{89}Zr-DFO-αCD11b. Retention of both agents in the liver was similar. There was greater residual radioactivity in the muscle, heart, thymus, lungs, and ipsilateral and contralateral hemispheres in mice receiving ^{89}Zr-DFO-αCD11b compared with ^{89}Zr-
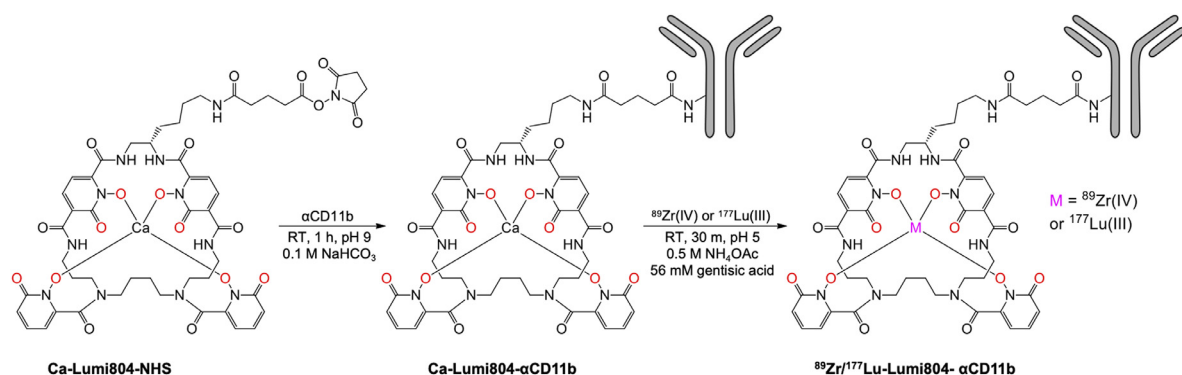
FIGURE 1. Structure of Ca-Lumi804-NHS and radiolabelling conditions. Reaction conditions for the preparation and radiolabelling of Ca-Lumi804-αCD11b. The eight oxygen atoms which bind the metal ion are shown in red, but only 4 coordination bonds are shown for clarity.

Lumi804-αCD11b. Overall, these data demonstrate reduced bone uptake of Zr-89 following administration of ^{89}Zr-Lumi804-αCD11b compared to ^{89}Zr-DFO-αCD11b, likely due to the ability of Lumi804 to form a more stable complex with Zr-89 than DFO.

Having established the improved long-term *in vivo* stability of ^{89}Zr-Lumi804-αCD11b, we then evaluated its utility for immunoPET imaging of TAMCs in glioma-bearing mice at 72 h post tracer injection (**Fig. 3a**). PET images, co-registered with MRI images with a transparency of 50% PET over MRI [34], verified tracer localization within the tumour (**Supplementary Fig. 4**). Consistent with our previous report using DFO [24], ^{89}Zr-Lumi804-αCD11b demonstrated significant uptake in the tumour-containing ipsilateral hemisphere (SUV_{mean} 1.4 ± 0.26) compared with the contralateral hemisphere (SUV_{mean} 0.21 ± 0.14; p<0.001, unpaired Student's t-test; **Fig. 3b**). To determine the specificity of ^{89}Zr-Lumi804-αCD11b for CD11b, a group of mice received agent that was 10-fold reduced in molar activity (i.e., a greater mass of Lumi804-αCD11b as a competitive block) (**Supplementary Fig. 5**). The group receiving agent with low molar activity showed significantly less uptake in the tumour ipsilateral hemisphere (SUV_{mean} 0.35 ± 0.29) compared with the non-blocked group (p<0.0001, unpaired Student's t-test; **Fig. 3b**). Conversely, no significant decrease in SUV was observed in the contralateral hemisphere of mice in the blocked group compared with non-blocked mice (p = 0.68; **Fig. 3b**). After confirming that the tumour accumulations were measurable with pre-clinical PET, we then determined the biodistribution of ^{89}Zr-Lumi804-αCD11b into dissected major organs at the point of PET imaging (72 h post tracer injection) to corroborate the observed PET data. We confirmed a significantly higher uptake of

^{89}Zr in the tumour ipsilateral hemisphere (3.4 ± 1.0 %ID/g) compared with blocked mice (1.3 ± 0.56 %ID/g; p<0.01, unpaired Student's t-test) and compared with the paired contralateral hemisphere (0.4 ± 0.2 %ID/g; p<0.01, unpaired Student's t-test; **Fig. 3c**). Significant differences were also noted in the contralateral hemisphere, blood, and lungs between the non-blocked and the blocked mice. No significant decreases were observed in the bone, muscle, liver, spleen, thymus, or intestine uptake between non-blocked and blocked mice (**Fig. 3c**). Due to high and variable blood activity, tumour-to-blood ratios were relatively low (T:B, 0.43 ± 0.32) but tumour-to-muscle ratios were higher (T:M, 5.5 ± 4.29). Our data suggest that tumour uptake of ^{89}Zr-Lumi804-αCD11b is likely reduced by high receptor-specific accumulation in peripheral organs such as blood. Future experiments, including a molar activity study would determine an optimal value to reduce receptor-mediated radiotracer uptake in blood, spleen, and other organs to improve tumour contrast.

Figure 3d and 3e show a time course of ^{89}Zr-DFO-αCD11b at 1, 24, 72, and 96 h, demonstrating rapid blood clearance by 48 h (SUV_{mean} = 0.46 ± 0.21) through 96 h (SUV_{mean} = 0.35 ± 0.15). Liver accumulation was relatively high, typical of an IgG-based radiotracer (SUV_{mean} = 0.89 ± 0.17, 72 h and SUVmean = 1.1 ± 0.50, 96 h). ^{89}Zr-Lumi804-αCD11b demonstrated significant uptake within GL261 tumour implants (72h post injection, SUV_{mean} = 0.52 ± 0.20) compared to contralateral brain (SUV_{mean} = 0.20 ± 0.87; p<0.05, unpaired Student's t-test). These values are consistent with the ratio of GL261 tumour accumulation to contralateral brain tissue (tumour: contralateral brain, 2.8 ± 0.6, 72 h). The tumour-to-blood ratios were highest at 72 h post injection (T:B, 1.8 ± 0.62, 72 h) but were moderated due to persistence of tracer in the blood. However, tumour-to-muscle ratios were high (T:M, 6.6 ± 7.0). We note a discrepancy in values in SUV_{mean} of the tumour and tumour:tissues ratios compared with the prior single timepoint PET (Figure 3a-c) experiment. In this experiment tumours grew more rapidly (determined by MRI) and higher interstitial pressures and vascular disruptions may have reduced tracer uptake.

3.3. ^{177}Lu-Lumi804-αCD11b has high tumour localization

While Zr-89 is a positron emitter suitable only for immunoPET imaging, Lu-177 is a β^- emitter which can kill target cells by TRT but provides poor *in vivo* visualization of tumour uptake by SPECT as the γ photons are in low abundance. To demonstrate tumour uptake of ^{177}Lu-Lumi804-αCD11b, SPECT/CT imaging of glioma-bearing mice was performed (7.4 MBq ^{177}Lu-Lumi804-αCD11b). We demonstrated greater uptake of ^{177}Lu-Lumi804-αCD11b in the tumour ipsilateral hemisphere (tumour site) compared with the contralateral hemisphere at 72 h post tracer injection (**Fig. 4a, b and Supplementary Fig. 6**). Immediately following SPECT/CT imaging, a biodistribution
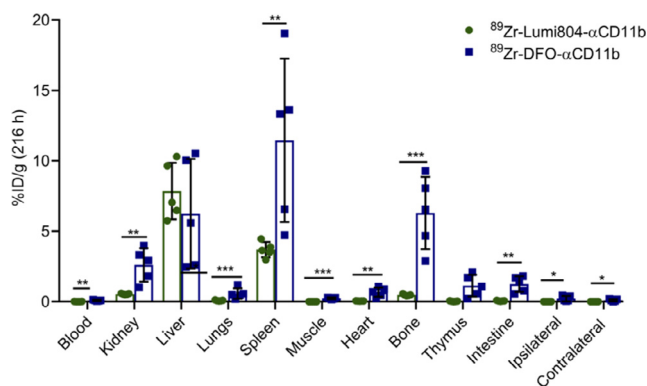

FIGURE 2. Lumi804 stably chelates Zr-89 resulting in low bone accumulation relative to DFO. Biodistribution analysis of ^{89}Zr-Lumi804-αCD11b and ^{89}Zr-DFO-αCD11b in major organs from glioma-bearing mice 216 h post-injection. Data are represented as the mean ± SD. (Unpaired t-test was used to assess significance).
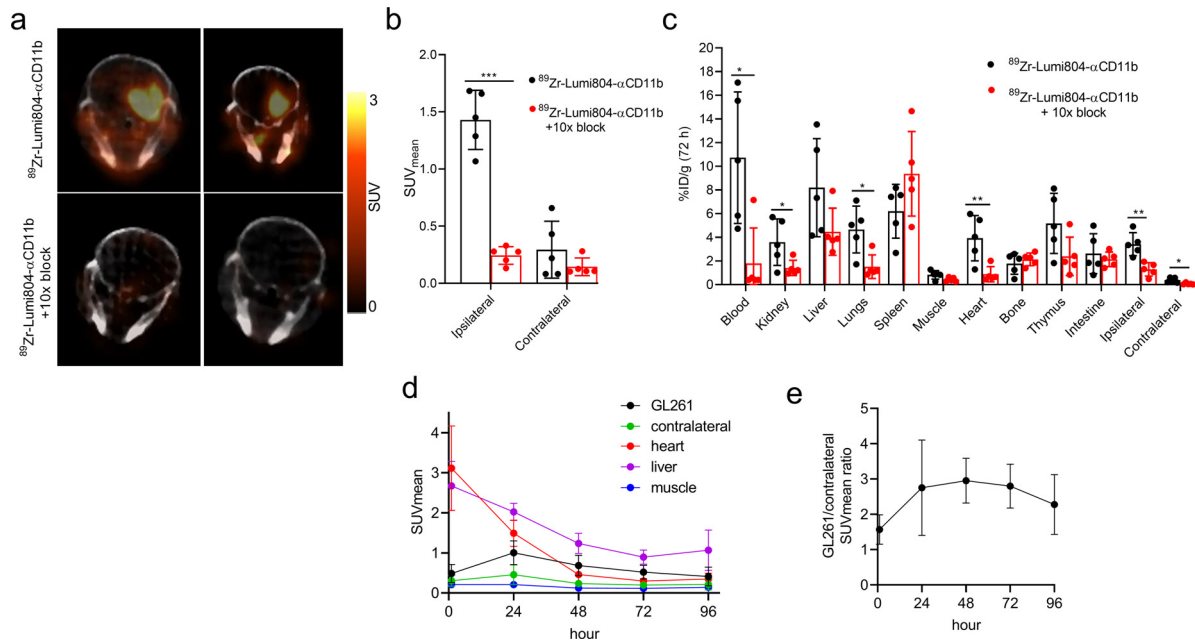
FIGURE 3. **^{89}Zr-Lumi804-αCD11b accumulation in glioma bearing mice is receptor mediated.** Glioma-bearing mice received injection of ^{89}Zr-Lumi804-αCD11b tracer alone or with 10x blocking dose ($n=5$/group). Mice were assessed at 72 h post-tracer injection. **(a)** Representative axial PET/CT images ($n=2$/group are shown). **(b)** Quantified SUV$_{mean}$ in tumour ipsilateral and contralateral hemisphere from both groups. **(c)** Biodistribution analysis of major organs. Data are represented as the mean $\pm$ SD; each data point represents a unique mouse. (Unpaired t-test was used to assess significance). **(d)** Biodistribution determined by ROI analysis (n=5) **(e)** Ratio of GL261 tumour accumulation to contralateral tissue.

analysis was performed to validate the observed higher uptake of the tracer in the tumour ipsilateral hemisphere (5.2 $\pm$ 0.27 %ID/g) relative to the contralateral hemisphere (0.71 $\pm$ 0.35 %ID/g; p<0.0001, paired Student's t-test; **Fig. 4c**). Significant uptake was noted in immune cell rich organs including spleen (34.1 $\pm$ 5.7 %ID/g) and thymus (10.2 $\pm$ 2.8 %ID/g) (**Fig. 4c**). Blood radioactivity was very low in all mice (0.01 $\pm$ 0.01 %ID/g), and consequently very high tumour-to-blood and tumour-to-muscle ratios were also observed (525 $\pm$ 270 and 69 $\pm$ 33, respectively). We speculate that the reason for the lower blood activity of ^{177}Lu-Lumi804-αCD11b relative to ^{89}Zr-Lumi804-αCD11b is due to eradication of CD11b-positive cells in the serum and subsequent liberation of the tracer from those cells for accumulation in liver and spleen, organs that are relatively resistant to radiation toxicity. The favourable biodistribution, rapid blood clearance, and high tumour ipsilateral hemisphere accumulation then led us to evaluate ^{177}Lu-Lumi804-αCD11b for TRT in glioma-bearing mice.

3.4. αCD11b TRT selectively depletes CD11b$^+$ cell populations and improves response to checkpoint inhibitor immunotherapy therapy

To determine whether a therapeutic dose of ^{177}Lu-Lumi804-αCD11b would decrease TAMCs in the spleen and tumour, glioma-bearing mice were treated with unlabelled αCD11b as a control (100 μg, n=5) or a single dose of Lumi804-αCD11b (100 μg) labelled with either 14.8 (n=4) or 22.2 (n=5) MBq of Lu-177. Five days post-TRT, tumours and splenocytes were isolated and analysed by flow cytometry for a panel of immune cell types. MDSCs and macrophages (CD11b-positive) were significantly reduced in the spleens of mice treated with ^{177}Lu-Lumi804-αCD11b (p<0.001, p<0.05, one-way ANOVA with Tukey's multiple comparisons test; **Fig. 5a**). Within the tumour, MDSCs were significantly reduced in mice treated with 22.2 MBq ^{177}Lu-Lumi804-αCD11b (p<0.05, one-way ANOVA with Tukey's multiple comparisons test), while TAMs trended downward (**Fig. 5b**).
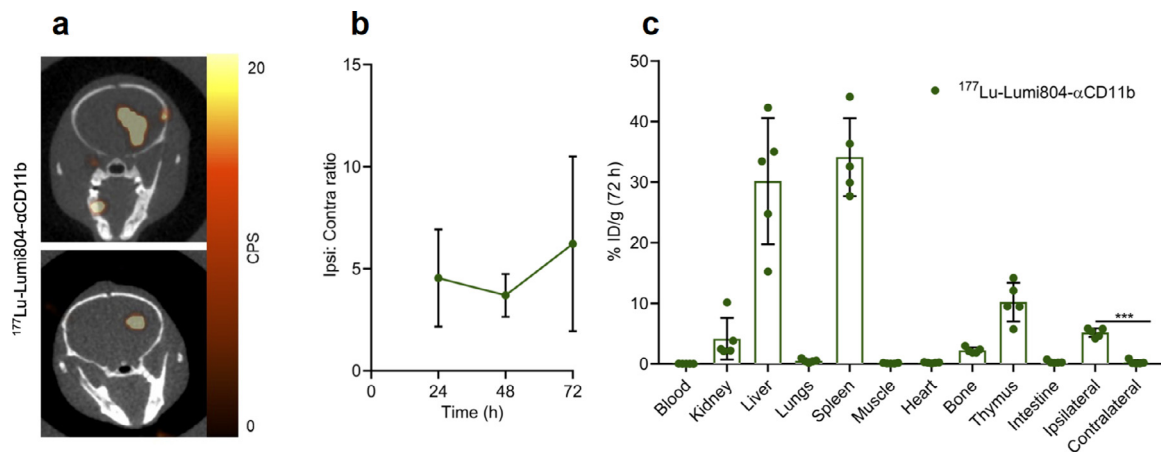

FIGURE 4. **^{177}Lu-Lumi804-αCD11b has high tumour accumulation. (a)** Representative axial SPECT/CT images ($n=2$) 72 h post-injection of ^{177}Lu-Lumi804-α-CD11b in glioma-bearing mice. SPECT signal scale from 0 to 20 counts per second (CPS). **(b)** Activity concentration ratio of tumour ipsilateral to contralateral hemisphere over time. **(c)** Biodistribution analysis of major organs from glioma-bearing mice 72 h post-treatment of ^{177}Lu-Lumi804-αCD11b. Each data point represents a unique mouse. Data are represented as the mean $\pm$ SD. (Paired t-test was used to assess significance).
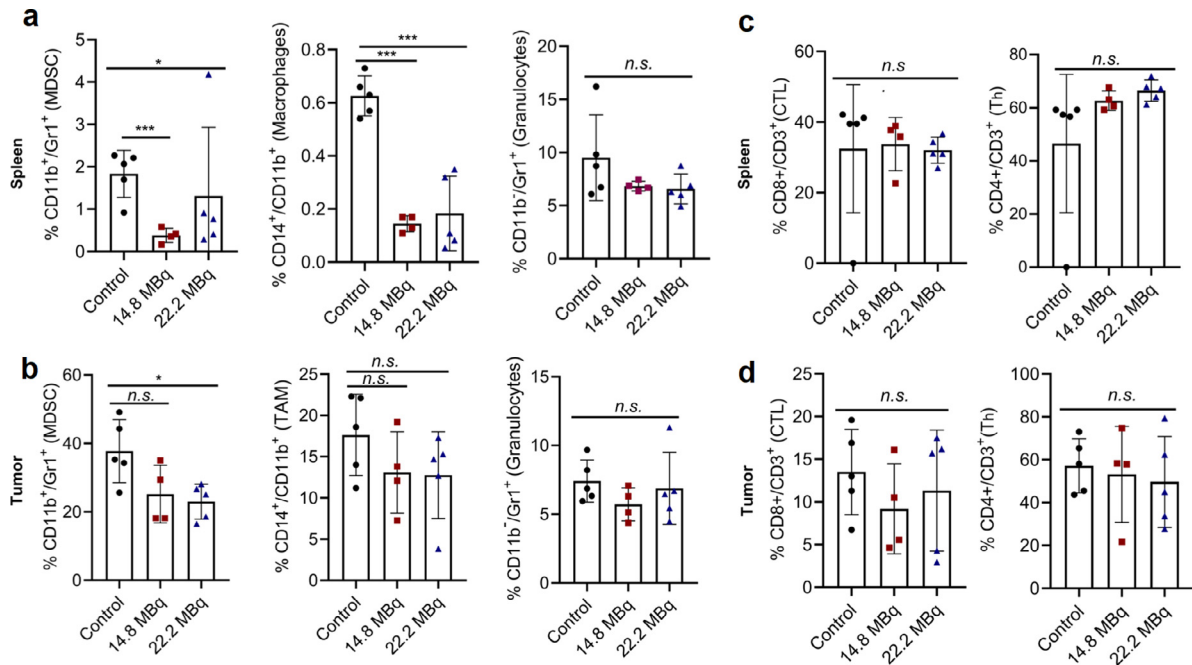
FIGURE 5. ^{177}**Lu-Lumi804-**α**CD11b TRT depletes CD11b$^+$ cells in the immune-periphery and within the TME.** Glioma-bearing mice were treated with αCD11b (control) or ^{177}Lu-Lumi804-α-CD11b TRT (either 14.8 MBq or 22.2 MBq). Spleen and tumour were harvested 5 days post-TRT, dissociated, and analysed by flow cytometry. **(a)** Myeloid cell populations, including MDSC, macrophages/TAM, and granulocytes, shown as a % of CD45$^+$ leukocyte-gated cells in spleen, and **(b)** in tumour. **(c)** Lymphoid cell populations, including CTL and T$_h$, shown as a % of CD45$^+$ lymphocyte-gated cells in spleen, and **(d)** in tumour. Data are represented as the mean ± SD. (One-way ANOVA with Tukey's multiple comparisons test was used to assess significance).

However, CD11b-negative cell populations (granulocytes, CD4$^+$ helper T-cells [T$_h$], and CD8$^+$ cytotoxic T-lymphocytes [CTLs]) in the spleen and tumour remained unchanged among treatment groups compared with cold antibody controls (**Fig. 5c, d**). Of note, no signs of therapy-related toxicity were apparent at time of autopsy.

While our data showed that CD11b$^+$ cells were more strongly depleted in lymphoid organs (e.g., spleen) following treatment with ^{177}Lu-Lumi804-αCD11b, even a moderate reduction in tumour infiltrating TAMCs or peripheral immunosuppression could improve

anti-tumour T cell responses and may therefore improve immunotherapy responses. Moreover, circulating monocytes, such as MDSCs and monocyte-derived dendritic-cells (DCs), could affect anti-tumour T cell responses through several mechanisms, including inhibiting T cell priming, maturation, and effector phenotype. Thus, we tested the ability of TRT to improve immunotherapy responses to checkpoint inhibitor immunotherapy (ICI; **Fig. 6**a), using a fractioned TRT dosing regimen (2 × 7.4 MBq) that we anticipated to maximize safety and therapeutic index. Importantly, we found that glioma-bearing mice
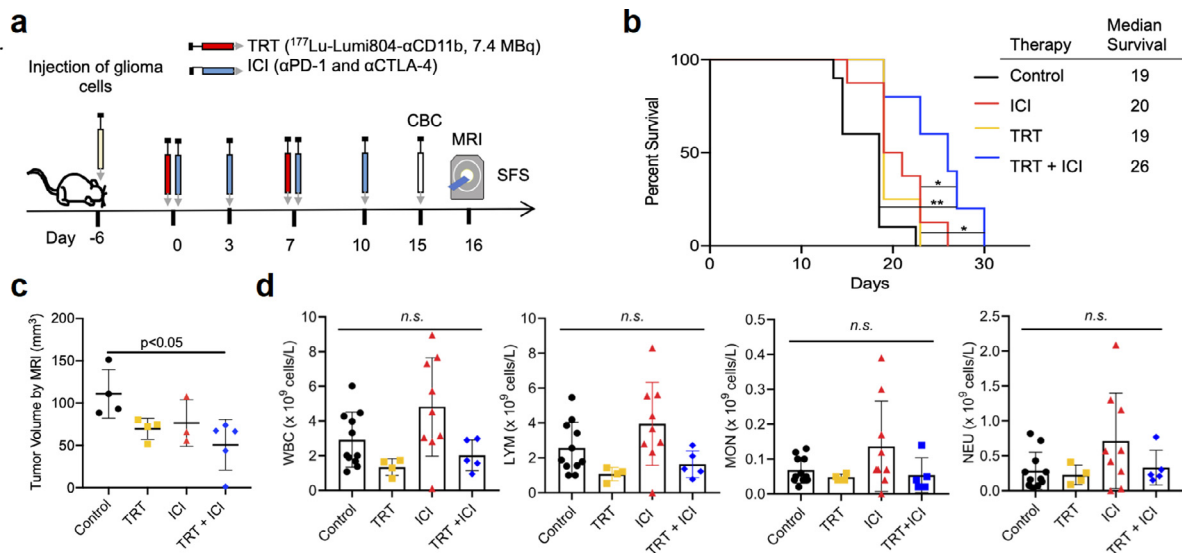

FIGURE 6. Combination TRT and ICI therapy in syngeneic glioma model reduces tumour volume and improves survival. (a) Schematic of survival study. **(b)** Kaplan-Meier survival curve of mice treated with vehicle (control, n=10), two doses of Lumi804-αCD11b (100 μg) labeled with 7.4 MBq Lu-177 (TRT, n=4; days 6 and 13 post-tumour cell injection), αPD-1 and αCTLA-4 antibody (ICI, n=8; days 6, 9, 13, and 16 post-tumour cell injection), or both TRT and ICI (n=5). X-axis indicates days post-initiation of therapy. Log-rank survival analysis was used to calculate p-values. **(c)** Quantification of tumour volume from MRI scans performed 16 days post-initiation of therapy. Unpaired t-test was used to assess significance. **(d)** CBC performed on superficial temporal vein blood 15 days post-initiation of therapy showed no leukodepletion from TRT. Data are represented as the mean ± SD. (One-way ANOVA with Tukey's multiple comparisons test was used to assess significance).

receiving a combination of TRT and ICI exhibited significantly prolonged survival (median SFS 26 days) compared with control (p<0.01, Kaplan Meier analysis with a log-rank test; median SFS 19 days), ICI only (p<0.05; Kaplan Meier analysis with a log-rank test, median SFS 20 days), or TRT only (p<0.05, Kaplan Meier analysis with a log-rank test; median SFS 19 days; **Fig. 6a-b**). Tumour volume, analysed by MRI, was reduced in glioma-bearing mice treated with combination TRT and ICI compared with control (p<0.05, one-way ANOVA with Tukey's multiple comparisons test; **Fig. 6c.**). Complete blood count (CBC) analysis demonstrated no leukodepletion in any treatment group or controls (**Fig. 6d, Supplementary Fig. 7**). Taken together, our data demonstrate that ^{177}Lu-Lumi804-αCD11b TRT can significantly improve αCTLA4/αPD1 immunotherapy and deplete CD11b$^+$ cells in both the immune-periphery and within the TME.

4. Discussion

Theranostics, the combination of targeted molecular therapy with diagnostic imaging, is an evolving field that encompasses nuclear medicine, radiation oncology, and medical oncology. Theranostics may be particularly well suited for malignant glioma patients, given the current lack of effective treatment options and current challenges in monitoring of therapeutic efficacy (e.g., tumour heterogeneity, treatment-response heterogeneity, and challenges acquiring tumour tissue for analysis). Development of theranostic agents for these tumours requires careful consideration of molecular targets and therapeutic radionuclides.

Radionuclide selection for theranostic pairing of agents must account for half-life that is suitable for the serum clearance of targeting agent, chelator compatibility, positron abundance for PET imaging, therapeutic efficacy, and availability of the radionuclide. Antibodies are highly effective targeting agents, but there is currently no chelator in widespread use which can rapidly and stably complex both Zr-89 and Lu-177, two of the most promising radiometals for an antibody-based theranostic. Previously reported Lu-177-labeled antibody conjugates primarily utilize DOTA or DOTA-derivatives as the chelator [35] [36], but the slow kinetics of Lu-177 incorporation into DOTA and DOTA-derivatives remain a significant challenge [37-44]. Furthermore, DOTA analogues do not bind Zr-89 under conditions that are suitable for antibodies. Previously reported Zr-89-labeled antibody conjugates primarily utilize DFO as the chelator, but DFO does not stably chelate Lu-177 and there remain significant stability issues for Zr-89 labelled DFO agents. Therefore, a single chelator that readily and stably binds both Zr-89 and Lu-177 under mild conditions is highly desirable for an effective antibody-based theranostic because it would facilitate translation of a single Lumi804-antibody immunoconjugate for FDA approval for both TRT and PET. The combination of Zr-89 (for PET) and Lu-177 (for TRT) is ideal for antibody-based theranostics due widespread availability and relatively long physical half-lives of these isotopes [26-29,45].

Here we utilize a newly developed macrocyclic BFC, Lumi804, which readily chelates metal ions that prefer 8-coordination, such as Zr(IV) and Lu(III). Our data demonstrate that Lumi804-αCD11b is radiolabelled with either Zr-89 or Lu-177 in 30 minutes at room temperature with high molar activity and high radiochemical yield (requiring no purification steps). The radiolabelled conjugates retained high immunoreactivity and demonstrated receptor specific accumulation in a preclinical animal glioma model. A significant concern of radiometal chelate incorporation into theranostics is bone deposition of free radiometal due to the instability of the chelate *in vivo*. Comparing the ^{89}Zr-Lumi804- and ^{89}Zr-DFO-αCD11b conjugates *in vivo*, the Lumi804 conjugate resulted in significantly less Zr-89 activity in the bone relative to the DFO conjugate, demonstrating the feasibility of Lumi804-radiolabeled conjugates for *in vivo* PET imaging of TAMCs.

Survival times for adults and children with malignant gliomas remain dismal [30], and an effective theranostic could be a highly attractive approach for treatment. TAMCs express CD11b on their surface and represent a major depot of immunosuppressive cells within gliomas that can directly promote tumour growth, angiogenesis, immunosuppression, immunotherapy resistance, and recruitment of immunoregulatory cells [9,10,46]. Our results showing tracer uptake within brain tumour are consistent with previous observations that GL261 tumours have a compromised BBB [47]. In the preclinical glioma model, used in this study stereotactic tumour injection allows rapid reestablishment of BBB integrity due to injection trauma within a week, and further damage to the BBB is physiologic from tumour growth [48,49]. Of note, circulating CD11b$^+$ myeloid-derived cells can migrate through the BBB into the CNS upon tissue damage [50-52], thereby facilitating transport of tracer-payload into the TME. Our data show that ^{177}Lu-Lumi804-αCD11b eradicates circulating CD11b$^+$ cells. As circulating CD11b$^+$ cells are immunosuppressive and migratory, this reduction may account for reduced numbers of these cells in the TME, and less immunosuppression within and outside the TME, leading to enhanced anti-tumour immunity. Together, these highlight a benefit of CD11b as a target, independent of BBB integrity. We recently demonstrated that an antibody-based immunoPET tracer ^{89}Zr-DFO-αCD11b had high receptor specific uptake within murine gliomas [22]. Following treatment with ^{177}Lu-Lumi804-αCD11b, we observed reductions of both MDSCs and CD11b$^+$ macrophages in splenocytes, while CD8$^+$ CTLs which are important for tumour cell killing, were not depleted. Furthermore, MDSCs were reduced in tumour samples, although to a lesser extent than in splenocytes. TAMs were the least affected by ^{177}Lu-Lumi804-αCD11b treatment, potentially due to their innate resistance to radiation, thus explaining their persistence in the TME [53]. Additionally, as oxygen is critical for TRT effectiveness [54,55], it is possible that TAMs are residing in hypoxic areas of the tumour. Moreover, lower radiation exposure in these poorly vascularized tumour regions may also contribute to greater reduction of splenic macrophages relative to TAMs [54,55]. An important future direction should explore radiosensitizing TAMs to further improve the efficacy of TAMC-targeted TRT.

While immunotherapies have proven remarkably effective in some cancer types, a large population of TAMCs contributing to an immunosuppressive TME has likely contributed to low efficacy of this treatment in glioma. Our demonstration that targeting TAMCs with ^{177}Lu-Lumi804-αCD11b in combination with ICI immunotherapy significantly prolongs animal survival shows the potential for TRT of TAMCs. Moreover, our TRT approach did not cause non-specific peripheral immune cell depletion (determined by CBC analysis) which is a significant element of safety for TRT. Moreover, immunosuppressive CD11b$^+$ myeloid cells, particularly MDSC, have been observed in many other types of cancers and are also a main target of immunotherapies [56,57]. Thus, our Lumi804-anti-CD11b could potentially be used as a theranostic agent in other types of CD11b$^+$ cell-enriched cancers.

A limitation of the current work is the remaining need to perform dosimetry for our tracers. Future dosimetry studies will allow for the prediction of off-target toxicity and safety due to tracer accumulation in organs such as the liver, due to IgG clearance, or spleen, given the presence of CD11b-positive cells. Off-target tracer accumulation is a common problem in TRT, ameliorated through dosimetric calculations to guide efficacious dosing. Bexxar, an I-I31-labeled antibody TRT agent for non-Hodgkin's lymphoma, demonstrated high liver and spleen accumulation, similar to our tracer. However, image-guided dosimetry determined a regimen for safe levels prior to treatment [58,59]. Similarly, we envision image-guided dosimetry with ^{89}Zr-Lumi804-αCD11b to set safe levels for ^{177}Lu-Lumi804-αCD11b. Advances in imaging technology, particularly in the clinical setting, such as the incorporation of cadmium-zinc-telluride (CZT) cameras

into modern SPECT are allowing for increased sensitivity and imaging speed to calculate dosimetry based upon ^{177}Lu-Lumi804-αCD11b, without the need for a separate PET radiotracer [60].

Some promising radiopharmaceuticals for radioimmunotherapy have been developed recently, such as the ^{177}Lu-labeled αPD-L1 antibody [61,62]. similarly, a synergistic effect was noted through TRT with a Lu-177-labeled peptide targeting $\alpha v\beta 3$ integrin in combination with anti-PD-1 checkpoint immunotherapy [63].

Here we report on the feasibility of Lumi804-αCD11b as a theranostic agent, with Lumi804 representing the first chelator readily complexing both Zr-89 and Lu-177 for immunoPET and TRT, respectively. To our knowledge, this is also the first report of a TRT or theranostic targeting immunosuppressive cells in any solid tumour. Utilizing Lumi804-αCD11 as a theranostic to reduce immunosuppression in combination with immune-stimulating therapies, while also allowing for immunoPET monitoring in glioma patients, may be a promising future clinical approach.

Contributors

Conceptualization: DM, CJA, WBE, GK.
Investigation: AF, SN, DST, JX, RK, EP, JDL, SV, BL, RG, LHM, IR, RE, MA, VP, LMF.
Writing-Original Draft: AF, SN, IR, DST, LHM, MA.
Writing-Review and Editing: IR, AF, SN, DST, IFP, AP, DM, RG, LMF, TKH, CJA, WBE, GK.
Supervision: TKH, RC, DM, CJA, WBE, GK.
All authors approved the final version of the manuscript.

Data sharing statement

Data of this study are available from the corresponding authors upon reasonable request.

Declaration of Competing Interest

DM, DST, and JX are employed and own stock options in Lumiphore, Inc. CJA is on the scientific advisory board and has funding from Lumiphore, Inc. GK receives research support from Lumiphore, Inc. All other authors have no conflict of interest in respect to the work presented in this manuscript.

Acknowledgements

Supplementary materials

Supplementary material associated with this article can be found, in the online version, at doi:10.1016/j.ebiom.2021.103571.

References

[1] Ostrom QT, Gittleman H, Truitt G, Boscia A, Kruchko C, Barnholtz-Sloan JS. CBTRUS Statistical Report: Primary Brain and Other Central Nervous System Tumours Diagnosed in the United States in 2011-2015. Neuro Oncol 2018;20 (suppl_4):iv1–iv86.

[2] Lamano JB, Lamano JB, Li YD, DiDomenico JD, Choy W, Veliceasa D, et al. Glioblastoma-Derived IL6 Induces Immunosuppressive Peripheral Myeloid Cell PD-L1 and Promotes Tumour Growth. Clin Cancer Res 2019;25(12):3643–57.

[3] Sarkar B, Paira P. Theranostic Aspects: Treatment of Cancer by Nanotechnology. Mini reviews in medicinal chemistry 2018;18(11):969–75.

[4] Yordanova A, Eppard E, Kürpig S, Bundschuh RA, Schönberger S, Gonzalez-Carmona M, et al. Theranostics in nuclear medicine practice. Onco Targets Ther 2017;10:4821–8.

[5] Hennrich U, Benešová M. [(68)Ga]Ga-DOTA-TOC: The First FDA-Approved (68)Ga-Radiopharmaceutical for PET Imaging. Pharmaceuticals (Basel) 2020;13(3):38.

[6] Hennrich U, Kopka K. Lutathera(R): The First FDA- and EMA-Approved Radiopharmaceutical for Peptide Receptor Radionuclide Therapy. Pharmaceuticals (Basel) 2019;12(3).

[7] Kamran N, Kadiyala P, Saxena M, Candolfi M, Li Y, Moreno-Ayala MA, et al. Immunosuppressive Myeloid Cells' Blockade in the Glioma Microenvironment Enhances the Efficacy of Immune-Stimulatory Gene Therapy. Mol Ther 2017;25(1):232–48.

[8] Kumar V, Patel S, Tcyganov E, Gabrilovich DI. The Nature of Myeloid-Derived Suppressor Cells in the Tumour Microenvironment. Trends Immunol 2016;37 (3):208–20.

[9] Perng P, Lim M. Immunosuppressive Mechanisms of Malignant Gliomas: Parallels at Non-CNS Sites. Front Oncol 2015;5:153.

[10] Won W-J, Deshane JS, Leavenworth JW, Oliva CR, Griguer CE. Metabolic and functional reprogramming of myeloid-derived suppressor cells and their therapeutic control in glioblastoma. Cell Stress 2019;3(2):47–65.

[11] Sica A, Porta C, Morlacchi S, Banfi S, Strauss L, Rimoldi M, et al. Origin and Functions of Tumour-Associated Myeloid Cells (TAMCs). Cancer Microenviron 2012;5 (2):133–49.

[12] Chen Y, Song Y, Du W, Gong L, Chang H, Zou Z. Tumour-associated macrophages: an accomplice in solid tumour progression. Journal of biomedical science 2019;26(1):78.

[13] Medina-Echeverz J, Aranda F, Berraondo P. Myeloid-derived cells are key targets of tumour immunotherapy. Oncoimmunology 2014;3:e28398.

[14] Hutter G, Theruvath J, Graef CM, Zhang M, Schoen MK, Manz EM, et al. Microglia are effector cells of CD47-SIRPalpha antiphagocytic axis disruption against glioblastoma. Proc Natl Acad Sci U S A. 2019;116(3):997–1006.

[15] Tamura R, Tanaka T, Ohara K, Miyake K, Morimoto Y, Yamamoto Y, et al. Persistent restoration to the immunosupportive tumour microenvironment in glioblastoma by bevacizumab. Cancer Sci 2019;110(2):499–508.

[16] Raphael I, Kumar R, McCarl LH, Shoger K, Wang L, Sandlesh P, et al. TIGIT and PD-1 Immune Checkpoint Pathways Are Associated With Patient Outcome and Anti-Tumour Immunity in Glioblastoma. Front Immunol 2021;12:637146.

[17] Pyonteck SM, Akkari L, Schuhmacher AJ, Bowman RL, Sevenich L, Quail DF, et al. CSF-1R inhibition alters macrophage polarization and blocks glioma progression. Nat Med 2013;19(10):1264–72.

[18] Qin H, Wei G, Gwak D, Dong Z, Xiong A, Kwak LW. Targeting tumour-associated myeloid cells for cancer immunotherapy. Oncoimmunology 2015;4(3):e983961.

[19] Cao Q, Huang Q, Mohan C, Li C. Small-Animal PET/CT Imaging of Local and Systemic Immune Response Using (64)Cu-alphaCD11b. J Nucl Med 2019;60 (9):1317–24.

[20] Cao Q, Huang Q, Wang YA, Li C. Abraxane-induced bone marrow CD11b(+) myeloid cell depletion in tumour-bearing mice is visualized by muPET-CT with (64) Cu-labeled anti-CD11b and prevented by anti-CSF-1. Theranostics 2021;11 (7):3527–39.

[21] Dmochowska N, Tieu W, Keller MD, Wardill HR, Mavrangelos C, Campaniello MA, et al. Immuno-PET of Innate Immune Markers CD11b and IL-1beta Detects Inflammation in Murine Colitis. J Nucl Med 2019;60(6):858–63.

[22] Nigam S, McCarl L, Kumar R, Edinger RS, Kurland BF, Anderson CJ, et al. Preclinical ImmunoPET Imaging of Glioblastoma-Infiltrating Myeloid Cells Using Zirconium-89 Labeled Anti-CD11b Antibody. Molecular imaging and biology 2019:1–10.

[23] Tatum D, Xu J, Magda D, Butlin N. Macrocyclic ligands with pendant chelating moieties and complexes thereof, WO/2019/173639, 2019: USA.

[24] Nigam S, McCarl L, Kumar R, Edinger RS, Kurland BF, Anderson CJ, et al. Preclinical ImmunoPET Imaging of Glioblastoma-Infiltrating Myeloid Cells Using Zirconium-89 Labeled Anti-CD11b Antibody. Mol Imaging Biol 2019.

[25] Minniti G, Muni R, Lanzetta G, Marchetti P, Enrici RM. Chemotherapy for glioblastoma: current treatment and future perspectives for cytotoxic and targeted agents. Anticancer research 2009;29(12):5171–84.

[26] van de Watering FC, Rijpkema M, Perk L, Brinkmann U, Oyen WJ, Boerman OC. Zirconium-89 labeled antibodies: a new tool for molecular imaging in cancer patients. BioMed research international 2014;2014:203601.

[27] Nayak TK, Brechbiel MW. Radioimmunoimaging with longer-lived positron-emitting radionuclides: potentials and challenges. Bioconjug Chem 2009;20(5):825–41.

[28] Zhang Y, Hong H, Cai W. PET tracers based on Zirconium-89. Curr Radiopharm 2011;4(2):131–9.

[29] Deri MA, Zeglis BM, Francesconi LC, Lewis JS. PET imaging with ^{89}Zr: from radiochemistry to the clinic. Nucl Med Biol 2013;40(1):3–14.

[30] Enríquez Pérez J, Kopecky J, Visse E, Darabi A, Siesjö P. Convection-enhanced delivery of temozolomide and whole cell tumour immunizations in GL261 and KR158 experimental mouse gliomas. BMC Cancer 2020;20(1):7.

[31] Szatmári T, Lumniczky K, Désaknai S, Trajcevski S, Hídvégi EJ, Hamada H, et al. Detailed characterization of the mouse glioma 261 tumour model for experimental glioblastoma therapy. Cancer Science 2006;97(6):546–53.

[32] X-z Ye, S-l Xu, Y-h Xin, S-c Yu, Y-f Ping, Chen L, et al. Tumour-Associated Microglia/Macrophages Enhance the Invasion of Glioma Stem-like Cells via TGF-β1 Signaling Pathway. The Journal of Immunology 2012;189(1):444–53.

[33] Heskamp S, Raavé R, Boerman O, Rijpkema M, Goncalves V, Denat F. (89)Zr-Immuno-Positron Emission Tomography in Oncology: State-of-the-Art (89)Zr Radiochemistry. Bioconjug Chem 2017;28(9):2211–23.

[34] Fedorov A, Beichel R, Kalpathy-Cramer J, Finet J, Fillion-Robin JC, Pujol S, et al. 3D Slicer as an image computing platform for the Quantitative Imaging Network. Magnetic resonance imaging 2012;30(9):1323–41.

[35] Niaz MJ, Batra JS, Walsh RD, Ramirez-Fort MK, Vallabhajosula S, Jhanwar YS, et al. Pilot Study of Hyperfractionated Dosing of Lutetium-177-Labeled Antiprostate-Specific Membrane Antigen Monoclonal Antibody J591 ((177) Lu-J591) for Metastatic Castration-Resistant Prostate Cancer. The oncologist 2020.

[36] Malenge MM, Patzke S, Ree AH, Stokke T, Ceuppens P, Middleton B, et al. (177)Lu-lilotomab satetraxetan has the potential to counteract resistance to rituximab in non-Hodgkin's lymphoma. Journal of nuclear medicine: official publication, Society of Nuclear Medicine 2020.

[37] Pérez-Malo M, Szabó G, Eppard E, Vagner A, Brücher E, Tóth I, et al. Improved Efficacy of Synthesizing *M(III)-Labeled DOTA Complexes in Binary Mixtures of Water and Organic Solvents. A Combined Radio- and Physicochemical Study. Inorganic chemistry 2018;57(10):6107–17.

[38] Price EW, Orvig C. Matching chelators to radiometals for radiopharmaceuticals. Chemical Society reviews 2014;43(1):260–90.

[39] Liu S. Bifunctional coupling agents for radiolabeling of biomolecules and target-specific delivery of metallic radionuclides. Advanced drug delivery reviews 2008;60(12):1347–70.

[40] De León-Rodríguez LM, Kovacs Z. The Synthesis and Chelation Chemistry of DOTA−Peptide Conjugates. Bioconjug Chem 2008;19(2):391–402.

[41] van der Meer A, Breeman WA, Wolterbeek B. Reversed phase free ion selective radiotracer extraction (RP-FISRE): a new tool to assess the dynamic stabilities of metal (-organic) complexes, for complex half-lives spanning six orders of magnitude. Applied radiation and isotopes: including data, instrumentation and methods for use in agriculture, industry and medicine 2013;82:28–35.

[42] Moreau J, Guillon E, Pierrard JC, Rimbault J, Port M, Aplincourt M. Complexing mechanism of the lanthanide cations Eu3+, Gd3+, and Tb3+ with 1,4,7,10-tetrakis(carboxymethyl)-1,4,7,10-tetraazacyclododecane (dota)-characterization of three successive complexing phases: study of the thermodynamic and structural properties of the complexes by potentiometry, luminescence spectroscopy, and EXAFS. Chemistry (Weinheim an der Bergstrasse, Germany) 2004;10(20):5218–32.

[43] Jang YH, Blanco M, Dasgupta S, Keire DA, Shively JE, Goddard WA. Mechanism and Energetics for Complexation of 90Y with 1,4,7,10-Tetraazacyclododecane-1,4,7,10-tetraacetic Acid (DOTA), a Model for Cancer Radioimmunotherapy. Journal of the American Chemical Society 1999;121(26):6142–51.

[44] Kostelnik TI, Orvig C. Radioactive Main Group and Rare Earth Metals for Imaging and Therapy. Chemical Reviews 2019;119(2):902–56.

[45] Tagawa ST, Milowsky MI, Morris M, Vallabhajosula S, Christos P, Akhtar NH, et al. Phase II study of lutetium-177−labeled anti-prostate-specific membrane antigen monoclonal antibody J591 for metastatic castration-resistant prostate cancer. Clinical cancer research 2013;19(18):5182–91.

[46] Porta C, Sica A, Riboldi E. Tumour-associated myeloid cells: new understandings on their metabolic regulation and their influence in cancer immunotherapy. FEBS J 2018;285(4):717–33.

[47] Cha S, Johnson G, Wadghiri YZ, Jin O, Babb J, Zagzag D, et al. Dynamic, contrast-enhanced perfusion MRI in mouse gliomas: correlation with histopathology. Magnetic Resonance in Medicine: An Official Journal of the International Society for Magnetic Resonance in Medicine 2003;49(5):848–55.

[48] Habimana-Griffin L, Ye D, Carpenter J, Prior J, Sudlow G, Marsala L, et al. Intracranial glioma xenograft model rapidly reestablishes blood-brain barrier integrity for longitudinal imaging of tumour progression using fluorescence molecular tomography and contrast agents. J Biomed Opt 2020;25(2):1–13.

[49] Arvanitis CD, Ferraro GB, Jain RK. The blood-brain barrier and blood-tumour barrier in brain tumours and metastases. Nat Rev Cancer 2020;20(1):26–41.

[50] Domingues P, Gonzalez-Tablas M, Otero A, Pascual D, Miranda D, Ruiz L, et al. Tumour infiltrating immune cells in gliomas and meningiomas. Brain Behav Immun 2016;53:1–15.

[51] Antonios JP, Soto H, Everson RG, Moughon D, Orpilla JR, Shin NP, et al. Immunosuppressive tumour-infiltrating myeloid cells mediate adaptive immune resistance via a PD-1/PD-L1 mechanism in glioblastoma. Neuro Oncol 2017;19(6):796–807.

[52] Piao Y, Liang J, Holmes L, Zurita AJ, Henry V, Heymach JV, et al. Glioblastoma resistance to anti-VEGF therapy is associated with myeloid cell infiltration, stem cell accumulation, and a mesenchymal phenotype. Neuro Oncol 2012;14(11):1379–92.

[53] Russell JS, Brown JM. The irradiated tumour microenvironment: role of tumour-associated macrophages in vascular recovery. Front Physiol 2013;4:157.

[54] Rockwell S, Dobrucki IT, Kim EY, Marrison ST, Vu VT. Hypoxia and radiation therapy: past history, ongoing research, and future promise. Curr Mol Med 2009;9(4):442–58.

[55] Graham K, Unger E. Overcoming tumour hypoxia as a barrier to radiotherapy, chemotherapy and immunotherapy in cancer treatment. Int J Nanomedicine 2018;13:6049–58.

[56] Wesolowski R, Markowitz J, Carson 3rd WE. Myeloid derived suppressor cells - a new therapeutic target in the treatment of cancer. J Immunother Cancer 2013;1:10.

[57] Law AMK, Valdes-Mora F, Gallego-Ortega D. Myeloid-Derived Suppressor Cells as a Therapeutic Target for. Cancer. Cells. 2020;9(3).

[58] Kaminski MS, Tuck M, Estes J, Kolstad A, Ross CW, Zasadny K, et al. 131I-tositumomab therapy as initial treatment for follicular lymphoma. New England Journal of Medicine 2005;352(5):441–9.

[59] Wahl RL. Tositumomab and 131I therapy in non-Hodgkin's lymphoma. Journal of Nuclear Medicine 2005;46(1 suppl):128S–40S.

[60] Chevalier E, Boursier C, Claudin M, Marie P-Y, Imbert L. Feasibility of 177Lu Therapy Monitoring Using Fast Whole-Body SPECT Recordings Provided by a High-Speed 360°CZT Camera. Clinical Nuclear Medicine 2020.

[61] Zhao X, Shao C. Radiotherapy-Mediated Immunomodulation and Anti-Tumour Abscopal Effect Combining Immune Checkpoint Blockade. Cancers (Basel) 2020;12(10).

[62] Ren J, Xu M, Chen J, Ding J, Wang P, Huo L, et al. PET imaging facilitates antibody screening for synergistic radioimmunotherapy with a 177Lu-labeled αPD-L1 antibody. Theranostics 2021;11(1):304.

[63] Chen H, Zhao L, Fu K, Lin Q, Wen X, Jacobson O, et al. Integrin αvβ3-targeted radionuclide therapy combined with immune checkpoint blockade immunotherapy synergistically enhances anti-tumour efficacy. Theranostics 2019;9(25):7948.